Science of the Total Environment 909 (2024) 168474

Contents lists available at ScienceDirect

Science of the Total Environment

journal homepage: www.elsevier.com/locate/scitotenv

Dryness stress weakens the sustainability of global vegetation cooling

Zilin Li [a,b], Xiaoyong Bai [b,c,e,f,*], Qiu Tan [a], Cuiwei Zhao [a], Yangbing Li [a], Guangjie Luo [d], Fei Chen [b,e], Chaojun Li [b], Chen Ran [b], Sirui Zhang [b], Lian Xiong [a,b], Fengjiao Song [b], Chaochao Du [a,b], Biqin Xiao [a,b], Yingying Xue [a,b], Minkang Long [b]

[a] School of Geography and Environmental Sciences, Guizhou Normal University, Guiyang 550001, Guizhou Province, China
[b] State Key Laboratory of Environmental Geochemistry, Institute of Geochemistry, Chinese Academy of Sciences, Guiyang 550081, China
[c] CAS Center for Excellence in Quaternary Science and Global Change, Xi'an 710061, Shanxi Province, China
[d] Guizhou Provincial Key Laboratory of Geographic State Monitoring of Watershed, Guizhou Education University, Guiyang 550018, China
[e] College of resources and environmental engineering, Guizhou University, Guiyang 550025, China
[f] College of Environment and Ecology, Chongqing University, Chongqing 404100, China

HIGHLIGHTS

- Cooling effect areas caused by vegetation greening are as follows 25.78 million km^2.
- In nearly 47 % of the area, the dryness stress will limit the greening of vegetation.
- Drought stress weakened the 10.8 % contribution of vegetation to the cooling effect.
- With 21.03 million km^2 of vegetation cooling effect were limited by drought stress.

GRAPHICAL ABSTRACT

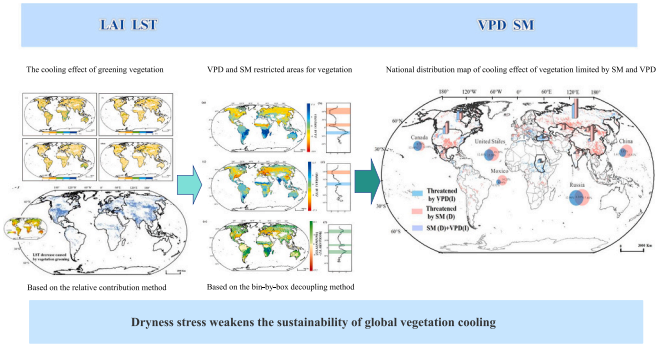

ARTICLE INFO

Editor: Anastasia Paschalidou

Keywords:
Soil moisture
Atmospheric vapor pressure deficit
Vegetation greening
Cooling effect
Sustainability

ABSTRACT

Dryness stress can limit vegetation growth, and the cooling potential of vegetation will also be strongly influenced. However, it is still unclear how dryness stress feedback weakens the sustainability of vegetation-based cooling. Based on the long-time series of multi-source remote sensing product data for the period 2001–2020, the relative contribution rate, and the method of decoupling and boxing, we determined that greening will likely mitigate global warming by 0.065 ± 0.009 °C/a, but nearly 47 % of the area is unsustainable. This phenomenon is strongly related to dryness stress. The restricted area of soil moisture (SM: 68.35 %) to vegetation is larger than that of the atmospheric vapor pressure deficit (VPD: 34.19 %). With the decrease in SM, vegetation will decrease by an average of 14.9 %, and with the increase in VPD, vegetation will decrease by 3.8 %. With the continuous increase in the dryness stress area, the sustainability of the vegetation cooling effect will be threatened in an area of about 21.03 million km^2, which is equivalent to the area of North America. Specifically, we found that with the decrease in SM and the increase in VPD, the contribution of vegetation to the cooling effect has been

* Corresponding author at: State Key Laboratory of Environmental Geochemistry, Institute of Geochemistry, Chinese Academy of Sciences, 99 Lincheng West Road, Guiyang 550081, Guizhou Province, China.
E-mail address: baixiaoyong@vip.skleg.cn (X. Bai).

https://doi.org/10.1016/j.scitotenv.2023.168474
Received 5 September 2023; Received in revised form 27 October 2023; Accepted 8 November 2023
Available online 10 November 2023

weakened by 10.8 %. This conclusion confirms that dryness stress will threaten the sustainability of vegetation-based climate cooling and provides further insight into the effect of dryness stress on vegetation cooling.

1. Introduction

Soil moisture (SM) and atmospheric vapor pressure deficit (VPD) are very important to the carbon cycle of terrestrial ecosystems. Some studies have found that SM-atmosphere feedback controls the change in soil carbon flux (Green et al., 2019). Low SM supply and high VPD are considered as the two main drivers of dryness stress on vegetation, which can cause large threats to agricultural production and drive widespread tree mortality (Madadgar et al., 2017). An accurate understanding of dryness stress on ecosystems is therefore critical for managing drought risks and reducing uncertainties in predicting future land carbon uptake and climate change(Liu et al., 2020; Liu et al., 2023b). SM and VPD infuence the distribution ratio of sensible heat and latent heat transmitted from the surface to the atmosphere, soil albedo, soil heat capacity, surface evaporation, and vegetation growth, which affect the redistribution of surface energy and water and thus the climate (Feng et al., 2021; Wang et al., 2010).

Vegetation is an indispensable part of the terrestrial ecosystem and plays an important role in water and energy cycle and information transmission (Seneviratne et al., 2010). Some scholars have shown that there is a significant greening trend for vegetation in China, India, southeastern Australia, and sub-Saharan Africa (Chen et al., 2019; Fridley and Wright, 2018). Peng et al. (2014) confirmed that this will produce an effective cooling effect. Peng et al. (2014) showed that the surface temperature in afforestation areas is lower than that in non-afforestation areas, which is attributed to the higher surface evapotranspiration (ET) caused by afforestation. Li et al. (2018) suggested that the mechanism of the vegetation cooling effect is mainly ET, which reflects the biophysical effect. Li et al. (2018) demonstrated that vegetation dynamics reflect the direct feedback of the environment to global climate change and human activities. In this system, they regulate the energy exchange among the atmosphere, water, and land(Dang et al., 2022; Deng et al., 2020; von Buttlar et al., 2018; Zhang et al., 2021). Many scholars have shown that several abiotic factors contribute to vegetation dynamics, including SM, VPD precipitation (Pre), and temperature (T) (Zheng and Eltahir, 1998). This proves that the interaction between SM and precipitation strongly affects the terrestrial water and energy cycle (McColl et al., 2017; Zhang et al., 2022b). It has been shown that the global soil drying trend is significant, and the response of vegetation change to soil drying is also significant (Castellvi et al., 1996; Jain et al., 2022). VPD is an important factor in vegetation dynamics. (Doughty et al., 2015; Liu et al., 2023a), and atmospheric drought and soil drying have negative effects on vegetation primary productivity (Mitchell et al., 2015; Song et al., 2020). The growth of vegetation is limited by SM and VPD (Zhang et al., 2022a), which may limit and threaten the resulting cooling effect. Feng et al. (2021) showed that the universality of vegetation greening is challenged and Will further affect the climate.The study of Green et al. (2019) showed that reduced SM can reduce the net primary productivity (NPP) and restrict the growth of vegetation through terrestrial ecosystem stress, which will further aggravate the occurrence of extreme climate due to terrestrial-atmospheric feedback. The research by Liu et al. (2023c) has shown that drought reduces evaporation and condensation, and the surface temperature in dry land increase compared with that in wet and marine areas. Therefore, the cooling effect of vegetation will be threatened and the surface temperature will rise in the soil drying areas and the atmospheric arid areas.Therefore, it is of great significance to pay attention to change in the cooling effect in vegetation regions, which is limited by a decrease in the SM and an increase in the VPD.

Although there have been many studies on the limitations of vegetation growth imposed by the SM and VPD, there are few studies on the relationship between SM and VPD and the cooling effect of vegetation, resulting in some shortcomings in our understanding::1. Can the extent by which SM and VPD limit the vegetation region be quantified in space? 2. Whether the effects of drought stress(SM and VPD) on vegetation will be further fed back to the atmosphere? 3. Is the cooling effect of vegetation is sustainable? 4. Is the indirect influence of SM and VPD on the cooling effect sustainable and what is the influencing mechanism?

Through several independent satellite observations of SM, VPD, Vegetation (leaf area index- LAI)、land surface temperature(LST), and contemporaneous climate data, first, we decouple the strong correlation between SM and VPD, and then solve their respective effects on limiting global ecosystem production and discuss the changes in the regional cooling effect that restrict vegetation growth. Our results show that compared with VPD, SM plays a leading role in determining the drought stress of ecosystem production in most terrestrial vegetation areas, and with the decrease in SM and the increase in VPD, the contribution of LAI to the cooling effect has been weakened by 10.8 % (Fig. 1).

2. Materials and methods

2.1. Date resource and preprocessing

2.1.1. Vegetation indices

Greening is quantified by LAI, while NDVI is usually used to indicate the dynamic change of vegetation. Compared with NDVI, the ecological significance of the leaf area index (LAI) is more obvious, that is, the total leaf area is projected on the unit land area(Sun and Qin, 2016). Therefore, the leaf area index (LAI) is a kind of vegetation index widely used for monitoring vegetation dynamics, and the LAI data set is a reliable "indicator" of vegetation interannual dynamics(Vickers et al., 2016). Peng et al. (2014) using the research results of the leaf area index, the vegetation greening is quantified. Data on vegetation leaf area index from 2001 to 2020 came from MODIS (https://disc.gsfc.nasa.gov/), with a spatial resolution of 500 m and a temporal resolution of 8 days. In order to match the precipitation and temperature data sets, we summarize the LAI data into monthly time steps.

2.1.2. Soil moisture data

In this paper, the monthly soil moisture data of 0.25 × 0.25 from 2001 to 2020 provided by NOAH, the land surface model of GLDAS is used(https://disc.gsfc.nasa.gov/), GLDAS, Global Land Surface Data Assimilation System, is developed jointly by the Goddard Space Flight Center of NASA and the National Center for Environmental Forecasting of the United States Oceanic and Atmospheric Administration (https://disc.gsfc.nasa.gov/). Based on surface observations and satellite remote sensing monitoring data, its four land surface process models including Noah have simulated SM products with various spatiotemporal resolutions(Roderick et al., 2007). This study adopted SM product from the Noah model, which contains four layers of SM data with depths of 0–10, 10–40,40–100, and 100–200 cm, respectively. In this paper, we mainly use soil moisture with a depth of 0-10 cm, unit: kg/m^2. GLDAS combines ground observation and satellite data products to generate optimal near-real-time ground state variables through data assimilation, which overcomes the limitations of ground. A lot of research and evaluation results show that GLDAS data has high reliability(Kato et al., 2007). At present, it has been widely used in the research fields of soil moisture research, remote sensing inversion of soil moisture results verification, climate and meteorological prediction, water resources management, drought, and flood disasters, etc.(Vreugdenhil et al., 2013).

2.1.3. Climate factors

Land Surface Temperature (LST) data in MODIS (https://disc.gsfc.nasa.gov/) products are used, which is the 8-day average data of LST from 2001 to 2021. The data of LST includes temperature observation during the daytime (10:30–13:30) and at night (22:30–01:30). The absolute deviation of noise LST caused by cloud pollution, topographic difference, and zenith angle change is <1 K.; Temperature and precipitation data are used for climate data, the global 0.5 climate data set (https://crudata.uea.ac.uk/cru/data/hrg/) published by CRU and the high-resolution climate data set (http://www.worldclim.org/) published by WorldClim.ET and Albedo data are homologous.VPD was calculated as the difference between saturated water vapor pressure, determined by near-surface temperature, and actual water vapor pressure, determined by saturated water vapor pressure and relative humidity.

2.1.4. Climate zone map

In this study, climate zones were defined according to the latest digital Köppen-Geiger World map of climate classification for the second half of the 20th century (Kottek et al., 2006), M. This map is based on data sets from the Climatic Research Unit(CRU TS2.1) at the University of East Anglia and the Global Precipitation Climatology Centre (GPCC) at the German Weather Service. (http://koeppen-geiger.vuwie- n.ac.at/present.htm).We merged the 31 climate zones into 5 major zones (Equatorial, Arid, Temperate, Boreal, Polar) as defined in the classificationsystem. The polar zone was not analyzed since it does not include relevant vegetated areas. We have to note here, that the climate zones are kept constant when doing statistics by climate zone even for future climate.See Fig. S2 Climatic Zone Classification Diagram for the specific classification diagram.

2.1.5. Global boundaries datasets

This study used different types of regional divisions for the world. Among them, global national vector boundary data (https://gadm.org/) and Köppen climate zone classification data (Kottek et al., 2006) were used. At the same time, in the process of quantifying the ecological threshold of SM and SFR on vegetation, the irrelevant variables should be control as much as possible.

The long-term multi-source remote sensing image data used in this paper are synthesized, aggregated, and cropped based on the source data, and the accuracy is unified by remote sensing software. In order to ensure the consistency of spatial resolution, ArcGIS was used to resample the above data.

2.2. Trend analysis

The Theil-Sen Slope and Mann-Kendall (MK) tests are less susceptible to outliers(Li et al., 2018). Therefore, this study combined the Mann-Kendall (MK) test and Theil-Sen median trend to analyze the spatio-temporal characteristics of LST, LAI, SM and various meteorological factors from 2001 to 2020. In this study, Theil-Sen Slope is considered significant when the absolute Z of the MK test is greater than or equal to 1.96. The MK test is a nonparametric test method (Hamed, 2008; Hamed and Rao, 1998; Libiseller and Grimvall, 2002).It often is combined with Theil- Sen slope estimation to detect the changing trend of long-term series data. The calculation formula is as follows:

$$\alpha = \frac{n\sum_{i=1}^{n}(i \times R_i) - \sum_{i=1}^{n} i \times \sum_{i=1}^{n} i \times \sum_{i=1}^{n} R_i}{n \times \sum_{i=1}^{n} i^2 - \left(\sum_{i=1}^{n}\right)^2} \quad (1)$$

where n is the research period, i represents the year number, and R_i is the value of the independent variable corresponding to the i- th year. α is a linear trend value, >0 represents an increasing trend, otherwise it represents a decreasing trend.

Define the Z statistic as:

$$Z = \begin{cases} \frac{S-1}{\sqrt{Var(S)}}, S > 0 \\ 0, S = 0 \\ \frac{S+1}{\sqrt{Var(S)}}, S < 0 \end{cases} \quad (2)$$

among them:

$$S = \sum_{j=1}^{n-1} \sum_{i=j+1}^{n} sign(R_j - R_i) \quad (3)$$

The sign function formula:

$$sign(R_j - R_i) = \begin{cases} 1, R_j - R_i > 0 \\ 0, R_j - R_i = 0 \\ -1, R_j - R_i < 0 \end{cases} \quad (4)$$

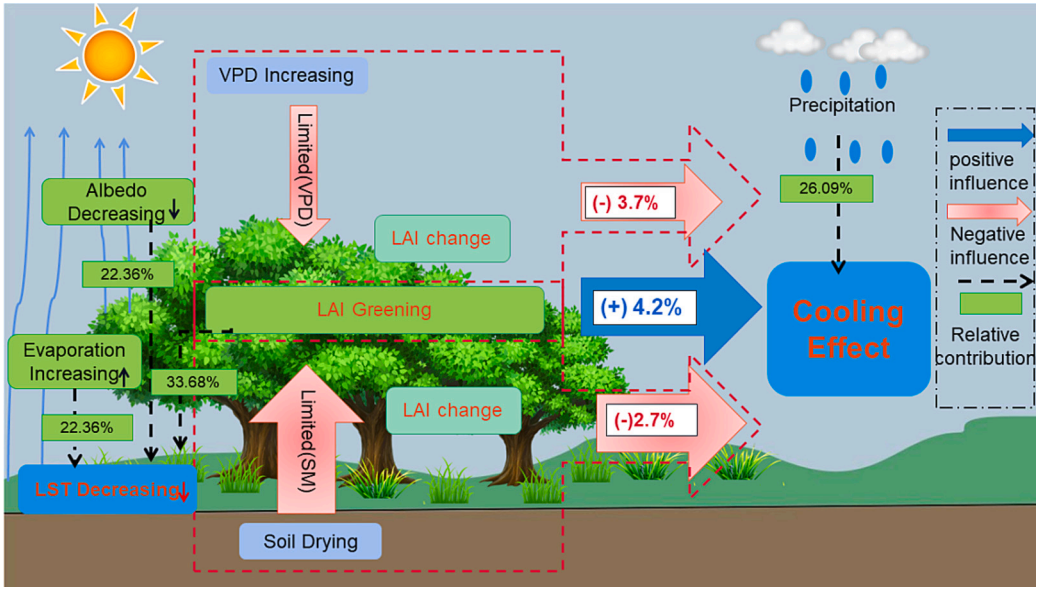

Fig. 1. Schematic diagram of the cooling effect of vegetation limited by SM and VPD. (The red arrow indicates the negative contribution value, he blue arrow is a positive contribution value, Green solid box is the relative contribution rate).

Var variance calculation formula:

$$Var(S) = \frac{n(n-1)(2n+5)}{18} \tag{5}$$

where sign is a sign function, this paper judges the significance of the change trend of the R factor at the significance level $p = 0.05$.

2.3. Correlation coefficient and partial correlation coefficient

In this paper, the correlation coefficient of GLDAS data of 0–10 cm soil moisture in China is calculated, and the correlation coefficients of LST and LAI with precipitation and temperature in time and space are also calculated. The specific calculation method is as follows:

$$r = \frac{\sum_{i=1}^{N}[(X_i - \overline{X})(Y_i - \overline{Y})]}{\sqrt{\sum_{i=1}^{N}(X_i - \overline{X})2\sum_{i=1}^{N}(Y_i - \overline{Y})2}} \tag{6}$$

In formula (6), X, Y,$\overline{X}$, and $\overline{Y}$ respectively represent two variables and the average value of variables, r is the correlation coefficient of variables, and n is the sample size.

Partial correlation analysis is called net correlation analysis, which is used to analyze the linear correlation between two variables under the condition of controlling the linear influence of other variables We used the method of (Huang et al., 2020). to determine the significance of each partial correlation, adjusted the p-value, determined the partial correlation information between the two factors on the pixel, and then used R to output the partial correlation. This study has 5 variables: LST LAI, Pre, ET, Abldo, the formula of the fourth–order sample partial correlation coefficient of any two variables LST and LAI is:

$$rlst.lai\_pre.Et.Abldo = \frac{rlst.lai\_pre.Et - rlst.Abldo\_pre.Et.rlai.Abldo\_pre.Et.}{\sqrt{(1 - rlst.Abldo\_pre.Et.^2)(1 - rlai.Abldo\_pre.Et.^2)}} \tag{7}$$

In formula (7), $.r_{\text{lst.lai\_pre,Et.Abldo}}$ represents the partial correlation coefficient between LST and LAI after removing the influence of the variables Pre, ET, and Abldo, $r_{\text{lst.Abldo\_pre,Et.}}$ and $r_{\text{lai.Abldo\_pre,Et}}$ represent respectively the correlation between LST and Abldo, LAI and Abldo after removing the influence of Pre and ET In addition, t–test is used to determine the significance of the correlation between the two variables, and if $p < 0.05$, the 95 % confidence significance test is passed, otherwise, it is not significant.

2.4. Assess the relative contribution of LAI and climate factors to LST

To analyze the relative contribution of SD, climate factors, and residual factors to LST changes,The method proposed by (Roderick et al., 2007) is used to estimate the relationship among LAI, pre, ET, Abldo and LST. This method has been widely used to evaluate the influence of various interference factors on hydrological and meteorological changes (Liu and Sun, 2016). we used the linear regression analysis (Liu et al., 2019) to calculate the actual LST trend. Taking the corresponding LST trend data as the dependent variable and each factor datum as the independent variable, the following equation is constructed:

$$\frac{dLST}{dt} = \frac{dLAI}{dt}\cdot\frac{\partial LST}{\partial LAI} + \frac{dET}{dt}\cdot\frac{\partial LST}{\partial ET} + \frac{dpre}{dt}\cdot\frac{\partial LST}{\partial pre} + \frac{dAbldo}{dt}\cdot\frac{\partial LST}{\partial Abldo} \tag{8}$$

$$= LAI\_Con + ET\_Con + pre\_Con + Abldo\_Con \tag{9}$$

where $\frac{d_{LST}}{dt}$ represents the Theil- Sen median trend of LST changes, $\frac{\partial_{LST}}{\partial_{LAI}}$, $\frac{\partial_{LST}}{\partial_{ET}}$, $\frac{\partial_{LST}}{\partial_{pre}}$, $\frac{\partial_{LST}}{\partial_{abldo}}$ represent the partial derivative values between LST and LAI, ET, PreandAbldo respectively. From the definition of the formula, each partial derivative eliminates the influence of the other two variables, and is equal to the corresponding second-order partial cor-relation coefficient,Con_LAI,Con_ET, Con_Pre, and Con_Abldo represent the contribution value of each factor to LST (Ge et al., 2021).

In order to separate the influence of LAI on LST from other influencing factors, we assume that other influencing factors remain unchanged, and use Pre, ET, Abldo and LAI data to quantify the contribution rate of climate change and vegetation to LST(Ge et al., 2021).The influence of hydro-climatic factors on LST is measured by constant climate simulation, so the relative contribution of hydro-climatic factors to LST is calculated as follows:

$$contr.lst = \frac{|\Delta lst.LAI|}{|\Delta lst.LAI| + |\Delta lst.pre| + |\Delta lst.ET| + |\Delta lst.Albdo|} \times 100\% \tag{10}$$

$$contr.lst. = \frac{|\Delta lst.pre|}{|\Delta lst.pre| + |\Delta lst.LAI| + |\Delta lst.ET| + |\Delta lst.Albdo|} \times 100\% \tag{11}$$

$$contr.lst = \frac{|\Delta lst.ET|}{|\Delta lst.ET| + |\Delta lst.pre| + |\Delta lst.LAI| + |\Delta lst.Albdo|} \times 100\% \tag{12}$$

$$contr.lst = \frac{|\Delta lst.Albdo|}{|\Delta lst.Albdo| + |\Delta lst.ET| + |\Delta lst.pre| + |\Delta lst.LAI|} \times 100\% \tag{13}$$

In the formula, contr,*lst* represents the contribution rate of climate and vegetation factors to LST. $\triangle lst$.LAI, $\triangle lst$.Albdo, $\triangle lst$.ET, $\triangle lst$.pre indicates the partial correlation coefficients between vegetation, reflectance, evapotranspiration and precipitation and surface temperature respectively.

2.5. Calculation of vapor pressure deficit

Monthly VPD (KPa) was calculated by subtracting the monthly actual water vapor pressure (AVP) from the monthly saturation water vapor pressure (SVP). SVP and AVP were calculated according to the Penman formula and the method recommended by (Ding et al., 2018),

$$\text{CRU}: \text{VPD} = \text{SVP} - \text{AVP} \tag{14}$$

$$\text{SVP} = 6.112 \times f_W \times e^{\frac{17.67T_a}{T_a+243.5}} \tag{15}$$

$$f_W = 1 + 7 \times 10^{-4} + 3.46 \times 10^{-6} P_{mst} \tag{16}$$

$$P_{mst} = P_{msl}\left(\frac{(T_a + 273.16)}{(T_a + 273.16) + 0.0065 \times Z}\right)^{5.625} \tag{17}$$

where Ta is the land air temperature (°C). Z is the altitude (m).P_{mst} is the air pressure (KPa), and P_{msl}l is the air pressure at mean sea level (101.325 KPa).

2.6. Decoupling of VPD and SM

In order to decouple the effects of SM and VPD, we used equal width binning as described by (Liu et al., 2020). The percentage SM per month was divided into ten intervals for each pixel (0 %–10 %, 10 %–20 %, 20 %–30 %, 30 %–40 %, 40 %–50 %, 50 %–60 %, 60–70 %, 70–80 %, 80 %–90 %, 90 %–100 %), and the difference between the highest VPD and the lowest VPD corresponding to the LAI for each interval was calculated and defined asΔLAI(VPD|SM):

$$\Delta\text{LAI}(\text{VPD}|\text{SM}) = \frac{1}{I}\sum_{i=1}^{I}\text{LAI}_{i,n_{i,max}} - \text{LAI}_{i,n_{i,min}} \tag{18}$$

where I is the number of populated SM bins, i is the specific SM bin number, and $n_{i,\max}$ and $n_{i,\min}$ are the maximum and minimum VPD bin numbers in SM bin $_i$. Equally, SM limitation on LAI without SM-VPD coupling (termed ΔLAI(SM|VPD)) was derived from the changes in LAI from high SM to low SM at each VPD bin as follows::

$$\Delta \mathrm{LAI}(\mathrm{SM}|\mathrm{VPD}) = \frac{1}{J}\sum_{i=1}^{J} \mathrm{LAI}_{j,m_{j,min}} - \mathrm{LAI}_{j,m_{j,max}} \quad (19)$$

where J is the number of populated VPD bins, j is the specific VPD bin number, $m_{j,max}$ and $m_{j,\ min}$ are the maximum and minimum SM bin numbers in VPD bin $_j$. The mean value of the bins was used to quantify the respective effects of SM and VPD on LAI.

To reveal the relationship between SM, VPD, and LAI, an equal-width binning method was used. When investigating the impact of SM on LAI, VPD was divided into 10 bins according to percentages, while SM and LAI also changed accordingly.based on binned averages, we fitted a linear regression between SIF and VPD in each SM bin. Consequently, the changes in LAI from lowest VPD bin to highest VPD bin from fitted linear functions were assigned as ΔLAI(VPD|SM). Likewise, SM stress in LAI (ΔLAI(SM|VPD) was also quantified.

2.7. Hurst index analysis and rescaling range analysis (R/S)

The Hurst index can quantitatively describe the degree of dependence of a sequence over a long period of time; so, it can be used to judge whether the future change in the sequence will be continuous. Then, the degree of continuity is described by classifying the numerical values. The assessment methods of the Hurst index mainly include the absolute value method, aggregate variance method, rescaled range (R/S)analysis method, periodogram method, Whittle method, residual variance method, and wavelet analysis. In this study, we use Hurst index to estimate the sustainability of SM, VPD and cooling effect, and use rescaled range (R/S) analysis method to study. Divide the long-term sequence (X_1,X_2.....,X_n) into S non-overlapping subsequences (X_{i1},X_{i2}…,X_{ij},i = 1,2,3, …,s,j = 1,2,3, …,r)of length r. The specific calculation steps are as follows:

(1) Time series mean $\overline{Xij}$

$$\overline{Xij} = \frac{1}{r}\sum_{j=1}^{r} Xij\,(\mathrm{i} = 1,2,3,\ldots,\mathrm{s},\mathrm{j} = 1,2,3,\ldots,\mathrm{r}) \quad (20)$$

(2) accumulative error Z_{ij},

$$Zij = \sum_{K=1}^{j}(Xij - \overline{Xij})\,(\mathrm{i} = 1,2,3,\ldots,\mathrm{s},\mathrm{j} = 1,2,3,\ldots,\mathrm{r}) \quad (21)$$

(3) extreme difference Ri,

$$\mathrm{R_i} = max\left(\mathrm{z_{ij}}\right) - min\left(\mathrm{z_{ij}}\right)(\mathrm{i} = 1,2,3,\ldots,\mathrm{s}) \quad (22)$$

(4) standard deviation Si,

$$Si = \sqrt{\frac{1}{r-1}\sum_{j=1}^{r}(Xij - \overline{Xi})2}\,(\mathrm{i} = 1,2,3,\ldots,\mathrm{s}) \quad (23)$$

(5) R/S,

$$RS = \frac{Ri}{Si}\,(\mathrm{i} = 1,2,3,\ldots,\mathrm{s}) \quad (24)$$

(6) and derive the Hurst index by fitting the formula H:

$$\mathrm{LogRS} = \mathrm{a} + \mathrm{H}^{*} log(\mathrm{n}) \quad (25)$$

The Hurst index can be divided into three categories. First of all, when the H index is between 0.5 and 1, the data series studied is a persistent series, that is, it has long-term correlation characteristics. The larger the H value, the stronger the persistence characteristics of the data series, the stronger the long-term memory of the data series, and the stronger the ability to keep the past state. Secondly, when H = 0.5, it shows that the data series studied is a random series, that is, there is no long-term correlation; The third category is when the H index is between 0 and 0.5, which indicates that the data series studied has anti-persistence, and its future change trend is opposite to the past change. The smaller the H value, the stronger the anti-persistence characteristics of the data series, which indicates that the data series has a stronger mutation. In this study, the Hurst index value is divided into three persistent categories: weak, medium , and strong, and the threshold values are 0 < 0.5, 0.5, and 0.5 < 1, respectively, for spatial analysis (Poveda, 2011).

3. Results and discussion

3.1. The cooling effect of vegetation greening

The confidence level of the MK test was 0.05, and the LAI and LST trend values were divided into five levels according to the standard (Table S1). We found that from 2000 to 2020, most parts of the world were mainly turning green (Fig. 2a), and that the green area was about 9309.25 × 10^4 km^2, accounting for 60.49 % of the total area. The most significant increase in LAI was concentrated in the northern hemisphere, especially in India and China (Chen et al., 2019). Although the global warming trend was obvious, the daytime surface temperature (LST) did not increase significantly in some areas where vegetation turned green, but there was a cooling effect, for example, in most tropical areas, temperate zones in the northern hemisphere, eastern Asia, and parts of the northern frigid zone (Table S2; Fig. 2b). In terms of climate zone classification, LST decreased significantly in tropical, temperate, and boreal areas. In an area of 5876.5 × 10^4 km^2, the LST decreased significantly; moreover, the area where LST decreased significantly was consistent with the trend of vegetation greening in areas where the LAI increased. While controlling precipitation and ET factors, the areas with a significant cooling effect that were affected by vegetation greening were mainly distributed in the northern hemisphere, concentrated mainly in tropical and temperate regions, and accounted for >50 % of the tropical and temperate regions (Fig. 2d). Precipitation (Pre) and evapotranspiration (ET) are important factors affecting LST, and they are also important mechanisms for LST to respond to vegetation changes (Yu et al., 2021). An increase in greening will affect the surface conditions and atmospheric circulation, reduce the surface albedo and air resistance power, and increase ET (Forzieri et al., 2020; Zeng et al., 2017). Partial correlation analysis showed that the LST in different regions is affected not only by LAI but also by other factors. Following the exclusion of factors based on partial correlation analysis, the vegetation greening trend map and cooling trend map were superimposed, and the cooling area caused by vegetation greening was obtained (Fig. 2c) (2577.75 × 10^4 km^2, accounting for 43.87 % of the cooling effect area). The greening rate of vegetation in this area was 0.207 ± 0.024 m^2/m^2, and the LST cooling rate was 0.065 ± 0.009 °C/a (Fig. S2).To further distinguish and quantify the relative contribution of each factor to LST in different regions, we performed a linear regression analysis pixel by pixel (Fig. 3a). On a global scale, LAI had the greatest influence (33.51 %) and was the most important factor controling the distribution and change in LST, which is consistent with previous research results (Roderick et al., 2007) that have reported similar influencing factors (Pre:26.09 % , ET:22.36 % , Albedo:20.65 %) (Fig. 3b). Although the factors were relatively close in the global scope, we found that the contribution rate of ET in tropical areas was significantly higher than that of Pre and closer to that of LAI, which is caused by the climatic background; In the temperate zone, the influence of LAI(48.3 %) was far greater than that of factors, and it was about 2.18 times that of precipitation (22.06 %), indicating that greening vegetation is an important factor of the cooling effect.

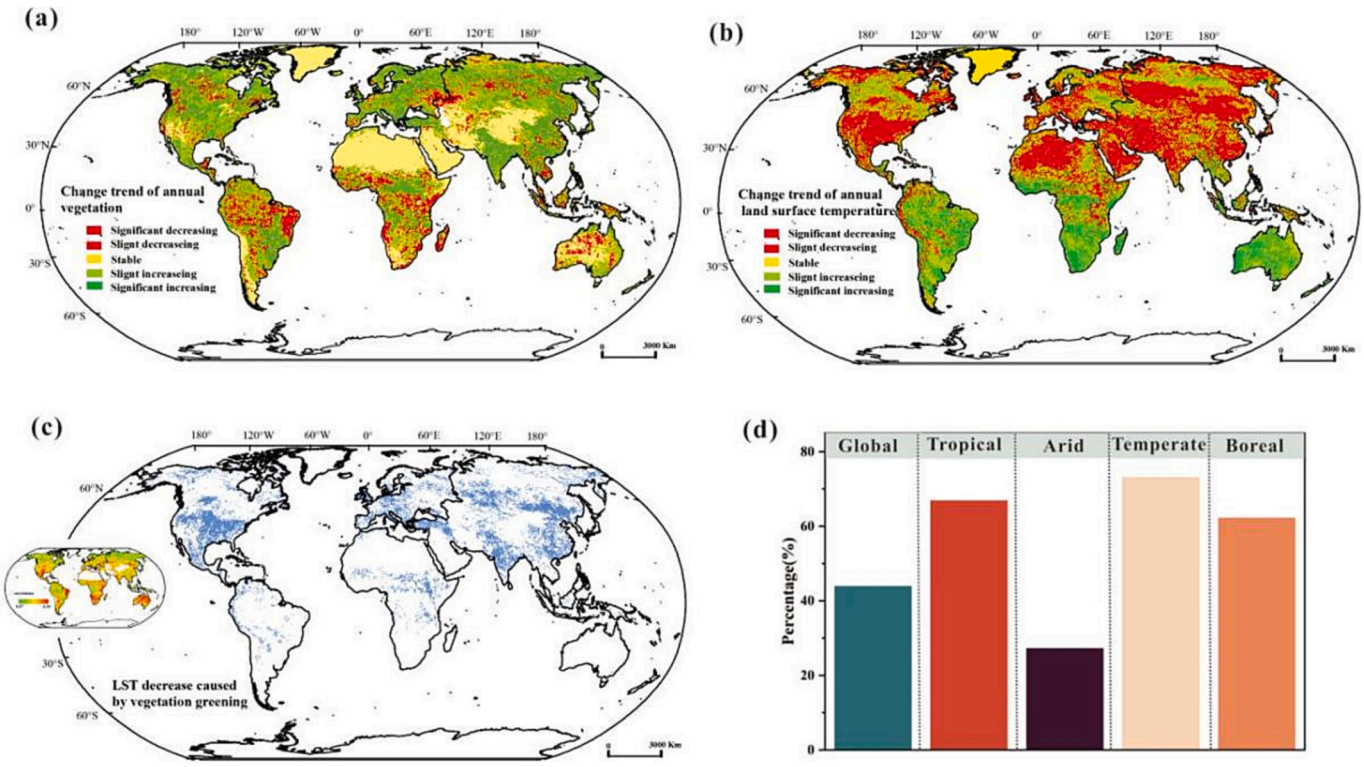

Fig. 2. Variation trend and correlation of vegetation and surface temperature from 2000 to 2020, and cooling effect area caused by greening vegetation. (a). (b) Annual variation trend of LAI and LST; (c) Represents the regional distribution map of cooling effect caused by vegetation greening, where the small graph represents the comparative correlation coefficient ($r > 0$,$r < 0$) and its relative significance level, where green and red are significantly and negative and positive respectively related area; (d) Represents the area percentage of the area with cooling effect of vegetation under the global climate division.

3.2. Influence of soil moisture and atmospheric vapor pressure deficit to vegetation

VPD measures the difference between SVP and AVP at air temperature, which can be used to indicate the impact of water stress on vegetation growth and is a key determinant of plant photosynthesis (Eamus et al., 2013). Soil moisture is the direct water source of vegetation, which determines the growth of vegetation. As shown in Fig. 4a, in 74 % of regions,SM is positively correlated with LAI, mainly in eastern Australia, sub-Saharan Africa, India and eastern Asia, and in 36 % of regions, SM is negatively correlated with LAI. Fig. 4b shows that VPD and LAI are negatively correlated in 81 % of regions, mainly in eastern Australia, sub-Saharan Africa, India and eastern Asia,and in 29 % of the regions, they are positively correlated. There is a strong negative correlation between SM and VPD in space (Fig. 4c), and the area with negative correlation between SM and VPD accounts for 89.32 % of the global land area(66.71 % of them had a regional correlation coefficient of <-0.3). Meanwhile, the difficulty in disentangling the respective effects of SM and VPD stems from the fact that SM and VPD are strongly coupled through land-atmosphere interactions (Seneviratne et al., 2010; Zhou et al., 2019). However, as SM and VPD are strongly coupled, it is possible that the correlation between SM and LAI is a byproduct of the correlation between VPD and LAI, or vice versa. As a consequence of SM-VPD coupling, the correlations of yearly SM and VPD with LAI are very similar globally (Fig. 3d). According to the above results, there is a strong coupling between SM and VPD on the annual scale. To clarify the influence of SM and VPD on vegetation change, it was necessary to decouple SM and VPD. From year to month (Fig. S3), the coupling largely remained across extensive areas, such as central South America, Sub-Saharan Africa, India, and Southeast Asia, which is consistent with previous findings(Liu et al., 2020). However, when binning the data into 10 bins according to percentiles of either SM or VPD per pixel, we found that the correlation coefficient between SM and VPD in each bin become approximately zero (Fig. S3). This shows that SM and VPD are generally decoupled at a monthly scale in both the SM and VPD bins. The changes in LAI from low VPD to high VPD without SM-VPD coupling (termedΔLAI(VPD|SM)) can quantify the VPD stress on LAI. Likewise, changes in LAI from high SM to low SM without SM-VPD coupling (termedΔLAI(SM|VPD)) can quantify the SM stress on LAI (Fig. 5a c). We found thatΔLAI(SM|VPD)) can is negative across most vegetated land areas, robustly indicating the limiting role of low SM to LAI (Fig. 5a b), wuich is understanding is consistent with previous research results (Seneviratne et al., 2010; Stocker et al., 2018). ΔLAI(SM|VPD)is mainly distributed in the northern hemisphere. But in terms of climate classification, it is mainly distributed in the temperate zone, arid zone and frigid zone of the northern hemisphere. In contrast, ΔLAI(VPD|SM) is smaller and closer to 0 in a large areas. However, ΔLAI(VPD|SM) accounts for a large proportion in tropical Africa around the equator (Fig. 5c d). Globally, a change from the wettest SM to the driest SM under constant VPD reduces LAI by up to 14.9 % on average, where the affected area accounts for 68.35 % of the world. And under stable SM, the average impact of the change from low VPD to high VPD on LAI (average decrease of 3.8 %) is less, with the affected area accounting for 34.19 % of the world.Locally, the areas where the strength of SM effects on LAI ($|\Delta$LAI(SM|VPD)$|$) exceeds that of VPD effects ($|\Delta$LAI(VPD|SM)$|$) are widespread, which is also visible along the latitudinal gradient (Fig. 5e,f). Generally speaking, in 68.35 % of the effective vegetation area, $|\Delta$LAI(SM|VPD)$|$ is greater than $|\Delta$LAI(VPD|SM)$|$; further,26.19 % of the regional vegetation is mainly restricted by VPD which has been confirmed by (Liu et al., 2020).

3.3. Comparison of vegetation cooling effects affected by soil moisture and atmospheric vapor pressure deficit

According to the linear regression model, the changing trend of SM and VPD from 2000 to 2020 has spatial heterogeneity (Fig. S4). The

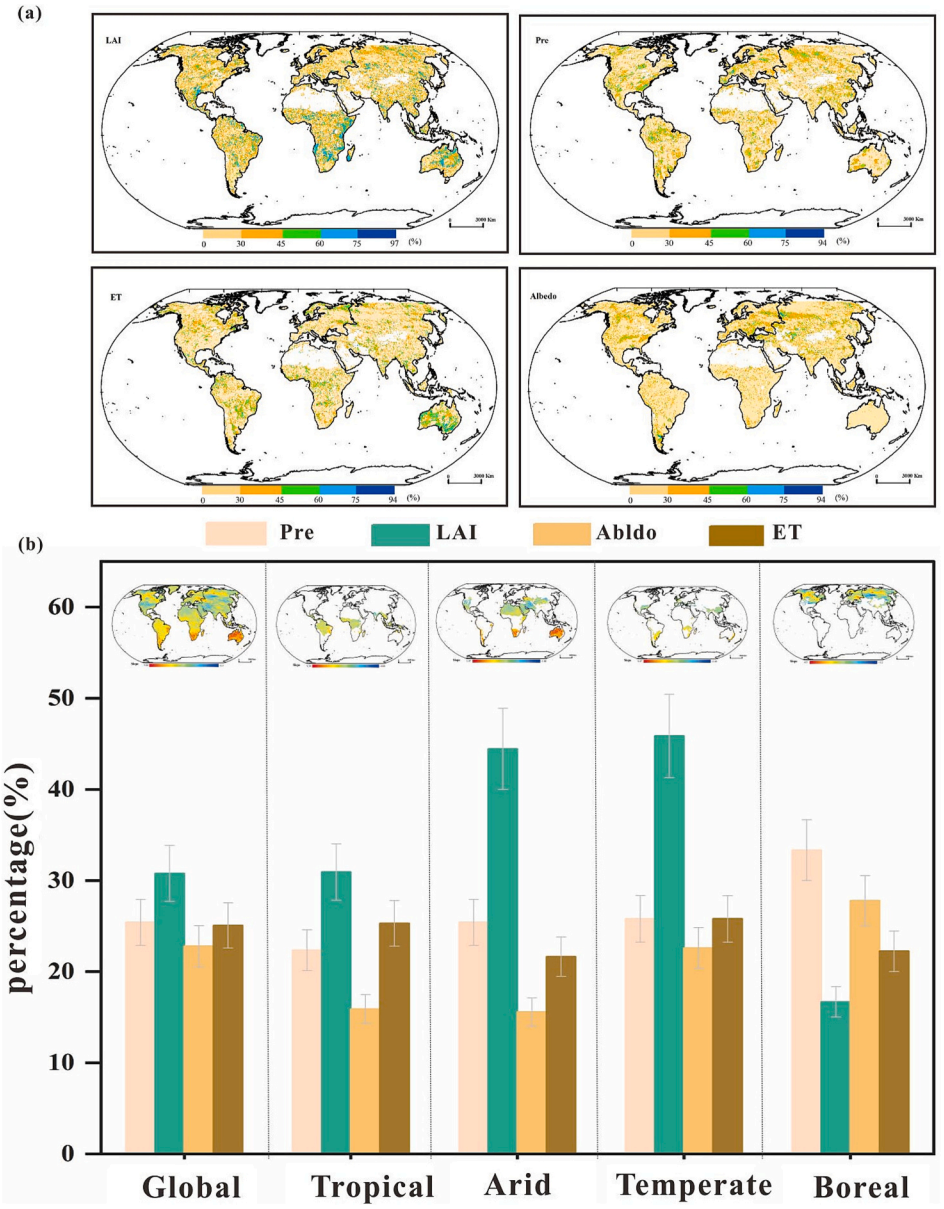

Fig. 3. Relative contribution rate of vegetation and climate factors to LST in global and climatic regionsAmong them. (a) the graph shows the relative contribution rates of LAI, Pre, Abledo and ET to LST on the global pixel scale, and (b) the graph shows the relative contribution rates of LAI, Pre, Abledo and ET to LST under global and climate zoning.

average annual decreasing trend of SM is significant, with a decrease rate of 0.13 ± 2.7 m^2/m^2, and the increasing trend of VPD is significant, with an increase rate of 0.12 ± 4.3 Kpa a^{-1}. As shown in Fig. S4b d, VPD is generally on the rise, accounting in 86 % of the global area, but in the southwest coastal areas of China, central South America and eastern Europe, it is declining; There is a decreasing trend in SM in 88 % of the global area, and these areas spatially overlap with the areas exhibiting an increasing trend in LAI (Fig. 2b). In summary, it has been preliminarily confirmed that SM and VPD have a restrictive effect on the growth of LAI, and the effect has been spatially quantified. The vegetation region limited by SM and VPD, was extracted and further analyzed with the cooling area caused by vegetation greening, and the change in the relative contribution rate of vegetation to the cooling effect is discussed below (Fig. 6).

The region with dry soil and restricted vegetation has an area of 3036.5×10^4 km^2, accounting for 32 % of the regional vegetation region. Globally, the negative contribution area is 74 %(We counted the sum of the positive and negative contribution areas in vegetation region, which is limited by low SM, as 100 %), and in terms of climate types, the negative contribution area in arid areas is as high as 91 % (Fig. 6b). This shows that a change in the SM in arid areas has a significant influence on vegetation change (Koster et al., 2004). The average contribution of LAI to LST in this area is 2.7 % (negative contribution to the cooling effect) (Fig. 6 a b). The area where VPD is increased and vegetation is restricted is 1981.25×10^4 km^2, and the average contribution of LAI to LST in this area is 3.7 % (negative contribution to the cooling effect) (Fig. 6b); On a global scale, the negative contribution area accounts for 64 %(We counted the sum of the positive and negative contribution areas in the vegetation region, which is limited by high VPD, as 100 %), and in terms of climate types, it is also the most negative contribution area in arid areas, accounting for 89 % of arid areas;, However, the negative contribution area of the northern boreal zone also accounts for a relatively large area, accounting for 82 % of the northern boreal region (Fig. 6 c d). This is consistent with the spatial increase of VPD in space, which shows that VPD is also an important factor that cannot be ignored in restricting the cooling effect of vegetation. In the cooling effect area

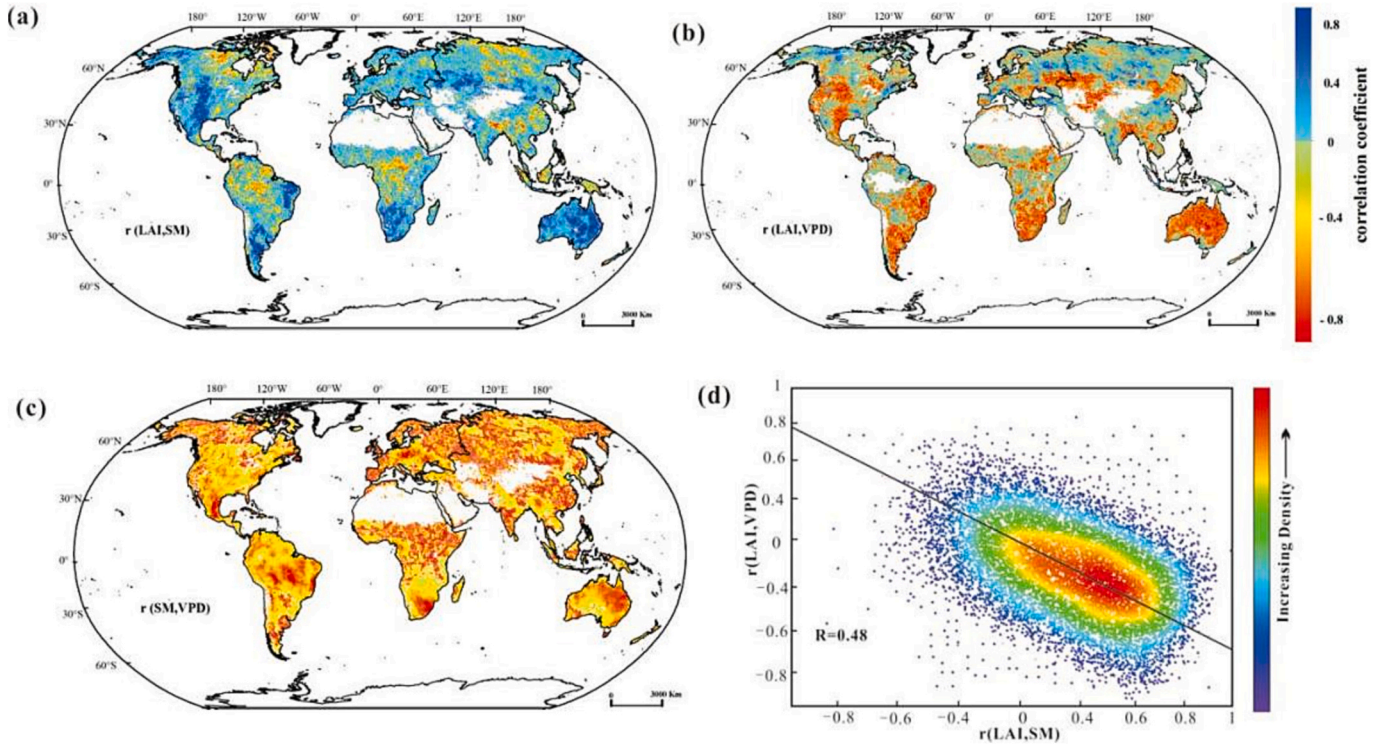

Fig. 4. Spatial distribution of correlation among soil moisture, atmospheric vapor pressure deficit and vegetation. (a) Correlation space diagram of LAI and SM; (b) Correlation space diagram of LAI and VPD; (c) Spatial distribution of correlation between SM and VPD; (d) The relationship between annual r(LAI, VPD) and annual r (LAI, SM) in the land vegetation area.

caused by vegetation greening, the contribution of vegetation to the cooling effect is −4.2 % (positive contribution to the cooling effect) (Fig. 6e). This proves that the change in SM and VPD weakens the positive contribution of LAI to the cooling effect of LST by about 10.8 %, and spatially, in >47 % of areas, soil drying and (VPD increase) atmospheric drought may limit the greening of vegetation, thus weakening the cooling effect and offsetting the cooling effect brought about by some vegetation.

3.4. Sustainability research on the dual limitation of SM and VPD on the cooling effect of vegetation

SM and VPD were analyzed using the Hurst coefficient (Fig. 7 a c). The area with SM coefficient >0.5 accounts for about 77 % of the total area, and the area with SM coefficient <0.5 accounts for about 23 % of the total area; The region with VPD coefficient >0.5 accounts for about 82 % of the total area, and the region with VPD coefficient <0.5 accounts for about 18 % of the total area. In combining these trends of SM and VPD with their correlation coefficients with LAI (Fig. 7 b d), it is found that the trend of decreasing SM and increasing VPD is more sustainable than anti-sustainable areas, which proves that the global trend of SM decrease and VPD increase will always be sustainable.The sustainability of this trend will also continue to threaten the greening of vegetation and limit the sustainability of its cooling effect. The strong correlation region of LAI and LST decrease was superimposed with the strong correlation and sustainable region of SM decrease and LAI decrease and the strong correlation and sustainable region of VPD increase and LAI decrease respectively (Fig. 8).The decrease in vegetation will lead to an increase in albedo and a decrease in precipitation, which will subsequently lead to the positive feedback of regional drought, and the decrease in precipitation caused by vegetation degradation will make the cooling effect unsustainable.The sustainability of the cooling effect of vegetation greening is limited by SM and VPD in an area of 2103×10^4 km^2, which accounts for 22.60 % of the vegetation greening area.

This part of the region is significantly distributed in the northern hemisphere temperate region, in the southern and southwestern regions of China(SM:55 $\times$ 10^4 km^2 ; VPD:5.8125 $\times$ 10^4 km^2)、Russia(SM:80.5 $\times$ 10^4 km^2 ; VPD:49.375 $\times$ 10^4 km^2)、India(SM:9.125 $\times$ 10^4 km^2 ; VPD:2.125 $\times$ 10^4 km^2)、Canada(SM:23.1875 $\times$ 10^4 km^2 ; VPD:29.3125 $\times$ 10^4 km^2)、Mexico(SM:10.75 $\times$ 10^4 km^2 ; VPD:3.375 $\times$ 10^4 km^2)、United States(SM:39.9375 $\times$ 10^4 km^2 ; VPD:23.625 $\times$ 10^4 km^2)and tropical countries in central Africa (Fig. 8). In China, 15.83 % of the areas are controlled by SM, 1.61 % by VPD and 5.83 % by SM and VPD. In Russia, 17.88 % of regions are controlled by SM, 12.96 % of regions are controlled by VPD, and 4.34 % of regions are jointly controlled by SM and VPD. In the United States, 18.20 % of regions are controlled by SM, 12.48 % of regions by VPD and 15.20 % of regions are controlled by SM and VPD. In Mexico, 14.20 % of the regions are controlled by SM, 4.32 % of regions are controlled by VPD and 6.84 % of regions are controlled by SM and VPD. In Canada, 12.88 % of the regions are controlled by SM, 13.68 % of regions are controlled by VPD and 8.78 % of regions are controlled by SM and VPD. This kind of vegetation reduction caused by soil drying and atmospheric drought restriction is strong and persistent, and this restriction cannot be ignored, as it will pose a great threat and challenge to the cooling effect.

4. Discussion

4.1. Effect of SM and VPD on vegetation greening

Our study found that the drought stress was significant, and the VPD increased significantly in about 64 % of regions, and the drying trend of SM accounted for 76.35%of the soil moisture area. This is because under the background of global warming, soil drying is serious, and the atmospheric saturation pressure difference is increasing, resulting in the continued expansion of arid areas (Deng et al., 2020; Yuan et al., 2019). The global arid areas have been expanding over the past 60 years and

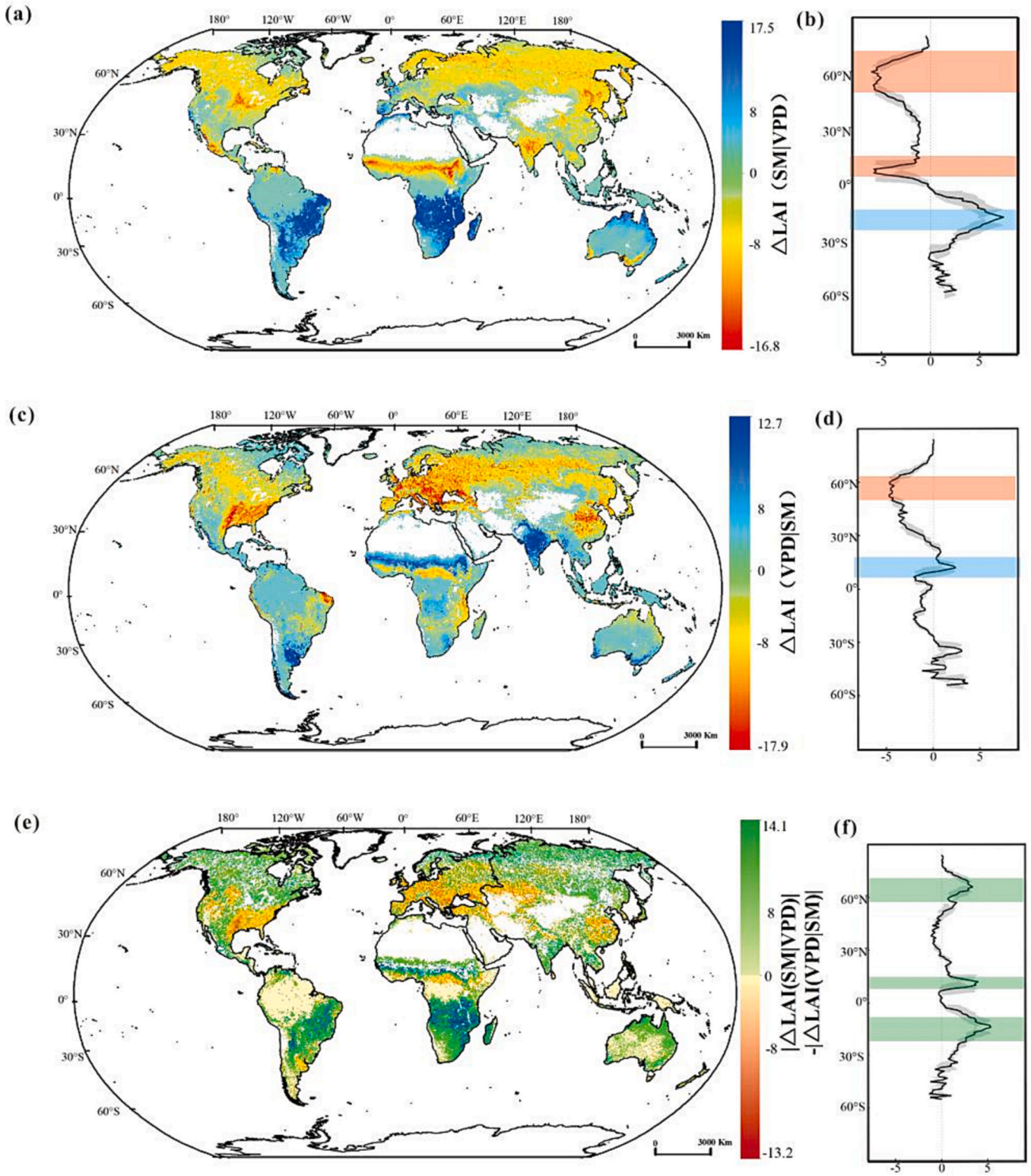

Fig. 5. Impact map of SM and VPD on global vegetation. (a). (c). (e) Spatial distribution of the changes in Leaf area index (LAI) caused by low soil moisture (SM) (ΔLAI(SM|VPD)) and high vapor pressure deficit (VPD) (ΔLAI(VPD|SM)), and their differences in absolute values (i.e., |ΔLAI(SM|VPD)| − |ΔLAI(VPD|SM)|); (b). (d). (f) Zonal means of SM and VPD effects on SIF and their differences in absolute values. The units refer to the fractions relative to average SIF exceeding the 90th percentile in each grid cell. Black lines indicate the mean values, and gray shaded bands show the standard deviation. Regions with sparse vegetation and regions without valid data are masked in white, colored bands indicate salient areas.

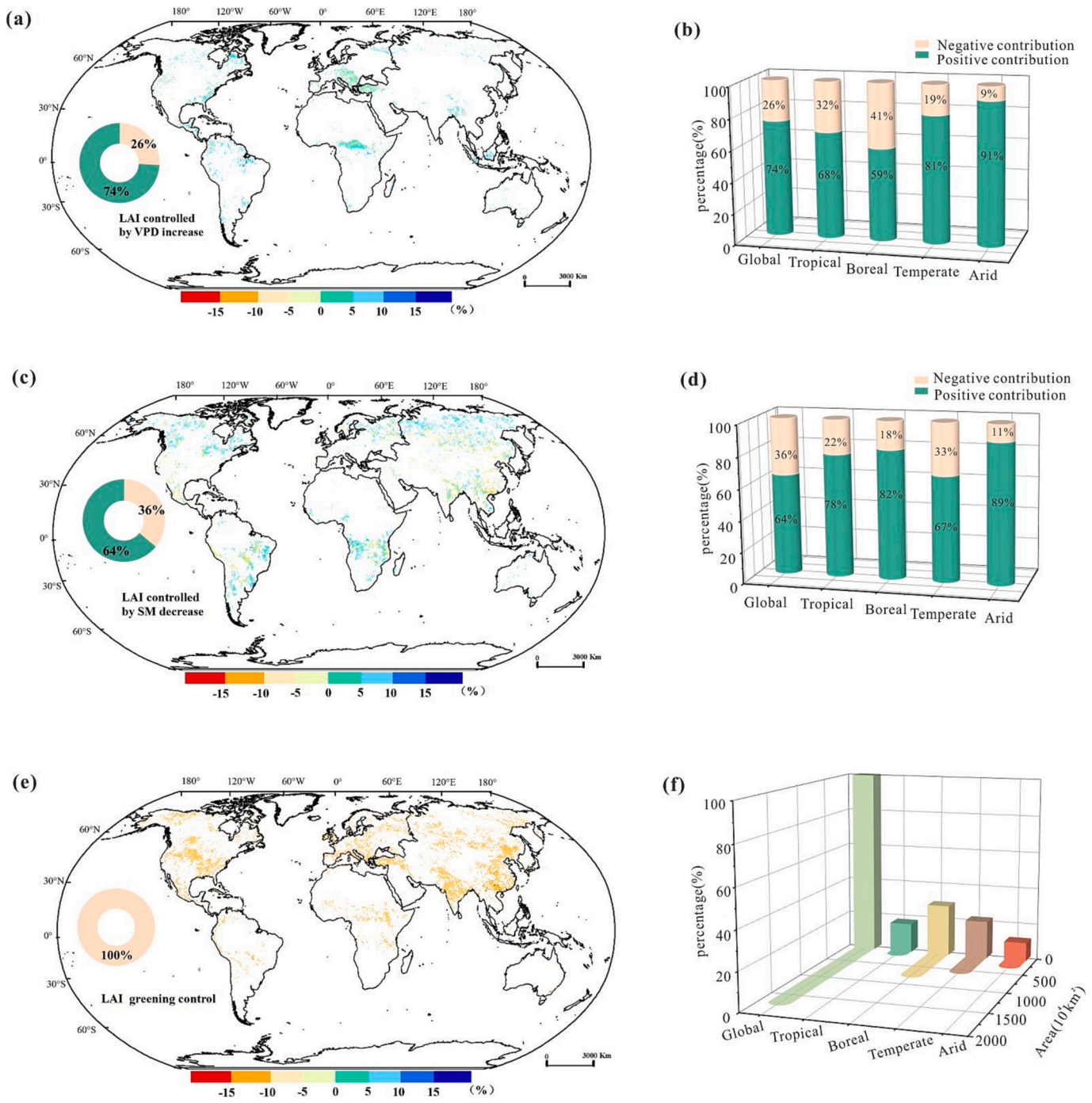

Fig. 6. Variation in the contribution rate of vegetation to the cooling effect in the vegetation region limited by soil moisture (SM) and atmospheric vapor pressure deficit(VPD). (a) Relative contribution of LAI in the vegetation region limited by high saturated pressure difference to LST and the proportion of positive and negative contributions, in which the area of vegetation limited by high saturated pressure difference is counted as 100 %. (c) Relative contribution rate and positive and negative contribution ratio of LAI to LST in the vegetation region with low soil water limitation, in which the vegetation area limited by low soil water is counted as 100 %. (e) Relative contribution of LAI to LST in the vegetation greening area. Green represents a positive contribution, that is, it promotes an increase in LST, and yellow represents a negative contribution, that is, it leads to a decrease in LST, but for the cooling effect, green is a negative contribution and yellow is a positive contribution; (b)&(d) Percentage of positive contribution and negative contribution to the study area in each climate division. (f) Proportion of area within the climate zone.

will continue to expand in the 21st century (Feng and Fu, 2013), and this drought stress is a direct threat to global vegetation (Madadgar et al., 2017). Low SM supply and high atmospheric saturation pressure difference are considered to be the two main driving factors of vegetation greening stress (Madadgar et al., 2017), which will lead to widespread tree death (Allen et al., 2010). This is because SM is the direct water source of vegetation, which determines the amount of water that can be extracted by plant roots, and thus, low precipitation and SM are typically used as indicators to measure the drought stress of vegetation (Stocker et al., 2018; Williams et al., 2010). High VPD may induce vegetation to close stomata to reduce water loss at the leaf surface scale and limit photosynthesis of plants (Oren et al., 1999). Furthermore, Yuan et al. (2019) demonstrated that the atmospheric saturated pressure difference (VPD) is the key variable that determines the photosynthesis

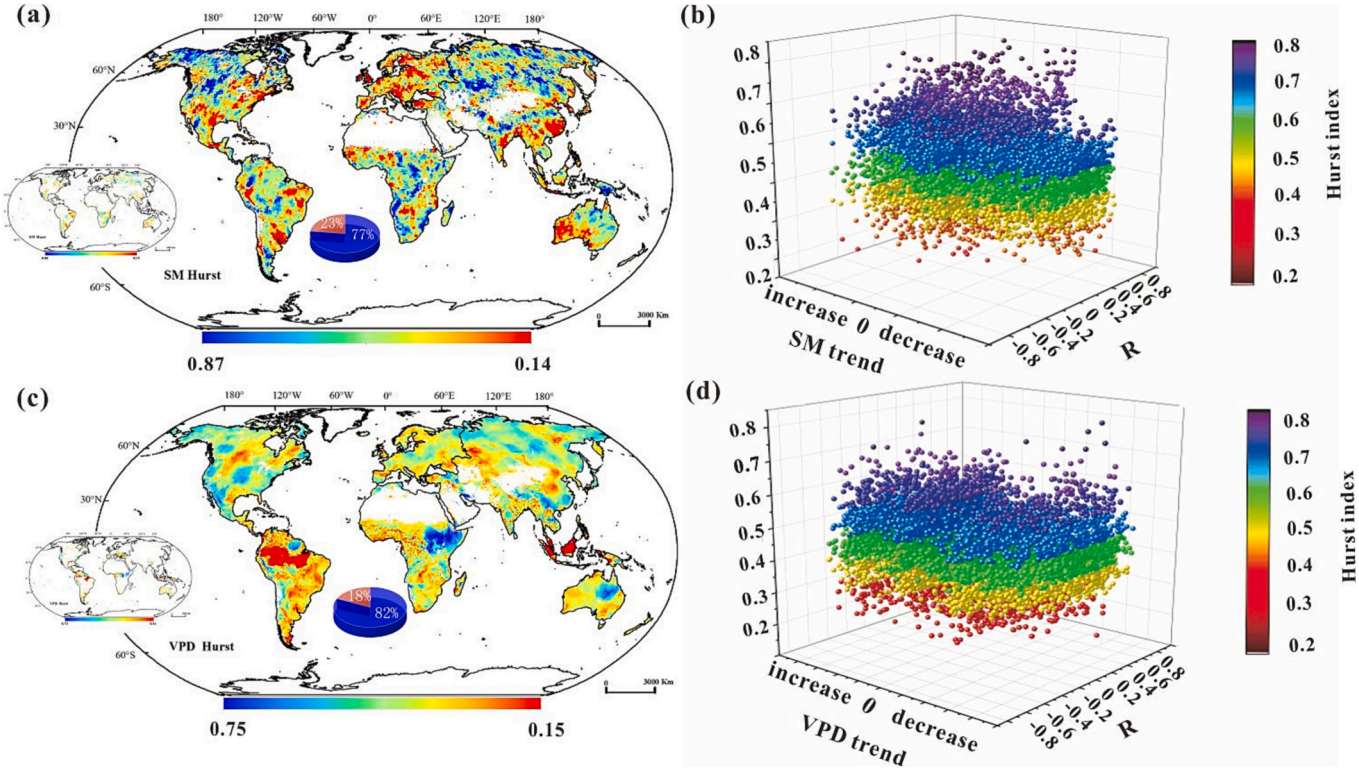

Fig. 7. Spatial-temporal distribution diagram of sustainability of SM and VPD. (a). (c).Represents the Hurst index distribution map of SM and VPD in vegetation region, in which the small map shows the SMHurst distribution map of the vegetation cooling effect area limited by soil water and the VPDHurst distribution map of the vegetation cooling effect area limited by VPD respectively,Pie charts represent percentage of area > 0.5,<0.5; (b). (d). Represents the relationship between their trend changes, Hurst index and correlation coefficient.

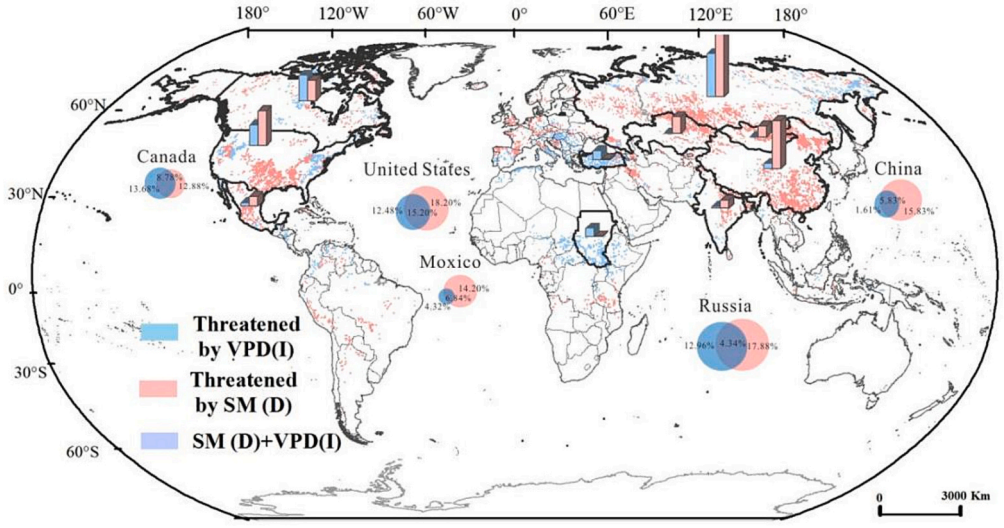

Fig. 8. National distribution map of cooling effect of vegetation limited by SM and VPD.(The bar graph represents the area and the circle graph represents the proportion).

of plants, and an increase in the atmospheric saturated pressure difference will limit the growth of vegetation. Seo et al. (2019) showed that soil drying may reduce or even exceed the potential benefits of temperature increase on photosynthesis.

Further, we found that SM and VPD are highly correlated, and there is an ongoing debate on the relative role of SM and VPD in determining the response of vegetation to dryness, because SM and VPD are coupled through the land-atmosphere interaction (Seneviratne et al., 2010; Zhou et al., 2019). Thus, we used the method of box decoupling to assess their individual effects (Liu et al., 2020). We found that compared with VPD, SM plays a leading role in determining the drought stress of most (68.35 %) of land vegetation regions. Low soil water has obvious restrictions on vegetation greening in mid-latitude areas, while high VPD has obvious restrictions in areas near the equator (Liu et al., 2020). In some tropical areas, SM and VPD have little influence on LAI because LAI is controlled by radiation and temperature (Nemani et al., 2003). The results of this study emphasize that soil drying and the increase in atmospheric saturated pressure difference will limit the greening of vegetation to

different degrees, and it is more conducive to clarify SM and VPD limiting role when considering SM-VPD coupling, which will introduce a new way to manage drought risk.

4.2. Comparative study on the sustainability limitation of the vegetation cooling effect caused by soil moisture and atmospheric vapor pressure deficit

Our research shows that the global trend of soil drying and atmospheric drought will significantly limit the greening of some vegetation and thus threaten the cooling effect in this region, and the cooling rate of surface temperature will slow down. With the decrease in SM and the increase in VPD, the contribution of vegetation to the cooling effect will be weakened by 10.8 %.

Soil drying and atmospheric drought threaten the sustainability of the cooling effect caused by vegetation greening, and this land-atmosphere interaction phenomenon is reflected at different research scales, whether regional or global(Baker et al., 2021; Sun and Qin, 2016). On a global scale, VPD is negatively correlated with vegetation growth. The global average VPD increased rapidly in the 20th century, which led to a slow decrease in the global average NDVI (Yuan et al., 2019). This is consistent with our research results, which show that the global VPD and LAI are significantly negatively correlated (Fig. 3b). In addition, the decrease in SM supply, coupled with high evaporation demand, leads to xylem vessel and rhizosphere cavitation (filled with air), stops the flow of water, dries plant tissues and leads to plant death (McDowell et al., 2008). Weisheimer et al. (2011) showed that under the background of global temperature rise and population increase, the trend of soil drying and atmospheric drought will be further aggravated, which will lead to more people being exposed to extreme heat waves, land degradation and other harsh environments. Green et al. (2019) confirmed that the difference between SM and VPD can reduce the total primary productivity (NPP) and limit vegetation growth through terrestrial ecosystem stress, which will further aggravate the occurrence of extreme climate due to land-atmosphere feedback. Furthermore, in terms of climate, we found that the cooling effect of vegetation greening exists (Fig. 2). This is because the continuous growth trend of LAI has contributed to the overall evaporation-driven cooling effect, especially in the arid and tropical environment with limited water resources (Forzieri et al., 2017). This cooling effect will be significantly affected by vegetation, that is, limited by drought stress, Zhou et al. (2021) showed that soil drying reduces evaporation and condensation, and the surface temperature on dry land will increase compared with that in wet and marine areas. Henderson-Sellers and Gornitz (1984) found that when the vegetation in the Amazon decreases, the surface reflectance increases and ET decreases, and the surface temperature will increases significantly, and the potential cooling effect is weaker than the warming effect. Consequently, deforestation in the Amazon basin will lead to an increase in the surface temperature. Zeng et al. (2017) used the land-air global climate coupling model (GCM) to quantify the response of global surface temperature change to vegetation greening over the past 30 years. The results showed that the cooling effect is not significant in eastern North America and East Asia. This is confirmed by the conclusions of our research. Due to the limitations of soil drying and atmospheric drought, the greening of vegetation is threatened, which limits the sustainability of the cooling effect in eastern North America and East Asia. Therefore, the influence of drought stress on the cooling effect should be further considered in the future ecosystem drought risk management.

4.3. Limitations of the study

In this study, the threats and limitations of soil drying and the increase in atmospheric saturated pressure difference on the sustainability of the vegetation cooling effect were evaluated, which promoted a deeper understanding of the driving mechanism of soil-vegetation-atmosphere interactions. However, our research has some limitations and uncertainties. First, in terms of SM data, we comprehensively considered several sets of data and found that the dataset considered in this study was the most suitable one, and thus, we only selected one set of soil moisture data for our research. Second, the growth and greening of vegetation will also be affected by other factors, but in this paper, SM and VPD are mainly discussed. In addition, in the research on the cooling effect, we mainly considered LAI, ET, Pre, and Albedo, and the total contribution rate of the four factors in this paper is assumed to be 100 %, because these four factors have been proven by many studies to be dominant in the influence on LST. Furthermore, the focus of this paper is on the influence of drought stress on vegetation in limiting the cooling effect. Other influencing factors require further study and need to be considered in future research, as well as the construction of more scientific models or the development of more effective methods to determine the causal relationship between vegetation and cooling effect. In view of these uncertainties and limitations, the next research will promote the dynamic computation of water-soil-bio-gas driving mechanism as one of the important tasks, so as to better understand the land-climate interaction mechanism on a global scale,These studies need to be carried out as soon as possible to provide a scientific basis for global drought risk management.

5. Conclusions

In this study, we used the box decoupling method, relative contribution rate method, linear regression model, and Hurst index analysis method to quantitatively evaluate the sustainable area of global soil drying and the effect of increasing atmospheric saturated pressure difference on the vegetation cooling effect. The main conclusions are as follows:

1) Vegetation is the most important contributor to the cooling effect, with a contribution rate of 33.51 %. The cooling effect area caused by vegetation greening is 2577.75×10^4 km^2 (accounting for 43.87 % of the cooling effect area), and the cooling rate in this area is 0.065 ± 0.009 °C/a.
2) The restricted area of SM (68.35 %) to LAI is larger than that of VPD (34.19 %). With a decrease in SM, LAI will decrease by 14.9 % on average, and with an increase in VPD, LAI will decrease by 3.8 % on average.
3) In nearly 47 % of the area, the dryness stress will limit the greening of vegetation. With the dryness stress, the contribution of LAI to the cooling effect has been weakened by 10.8 %.
4) The sustainability of the cooling effect of vegetation greening is limited by SM and VPD, and the area is 2103×10^4 km^2.

CRediT authorship contribution statement

Zilin Li: Conceptualization, Formal analysis, Writing – original draft. **Xiaoyong Bai:** Conceptualization, Supervision, Resources. **Qiu Tan:** Validation, Project administration. **Cuiwei Zhao:** Validation, Project administration. **Yangbing Li:** Validation, Project administration. **Guangjie Luo:** Validation, Project administration. **Fei Chen:** Validation, Formal analysis. **Chaojun Li:** Data curation, Writing – review & editing. **Chen Ran:** Data curation, Writing – review & editing. **Sirui Zhang:** Data curation, Writing – review & editing. **Lian Xiong:** Validation, Formal analysis. **Fengjiao Song:** Validation, Formal analysis. **Chaochao Du:** Visualization. **Biqin Xiao:** Validation, Formal analysis. **Yingying Xue:** Visualization. **Minkang Long:** Visualization.

Declaration of competing interest

The authors declare no competing interests.

Data availability

Data will be made available on request.

Acknowledgments

This research work was supported by National Natural Science Foundation (No.U22A20619 & No.42077455 & No.42367008), Western Light Cross-team Program of Chinese Academy of Sciences (No.xbzg-zdsys-202101), Strategic Priority Research Program of the Chinese Academy of Sciences (No.XDB40000000 & No.XDA23060100), Guizhou Provincial Science and Technology Projects (No.Qiankehe Support [2023] General 219 & [2023] Key 010, No.ZK(2021)-192), High-level Innovative Talents in Guizhou Province (No.GCC[2022]015-1 & No.2016-5648), Guizhou Provincial Science and Technology Subsidies (No.GZ2019SIG & No.GZ2020SIG).

Appendix A. Supplementary data

Supplementary data to this article can be found online at https://doi.org/10.1016/j.scitotenv.2023.168474.

References

Allen, C.D., Macalady, A.K., Chenchouni, H., Bachelet, D., McDowell, N., Vennetier, M., et al., 2010. A global overview of drought and heat-induced tree mortality reveals emerging climate change risks for forests. For. Ecol. Manage. 259, 660–684.
Baker, J.C.A., de Souza, D.C., Kubota, P.Y., Buermann, W., Coelho, C.A.S., Andrews, M. B., et al., 2021. An assessment of land-atmosphere interactions over South America using satellites, reanalysis, and two global climate models. J. Hydrometeorol. 22, 905–922.
von Buttlar, J., Zscheischler, J., Rammig, A., Sippel, S., Reichstein, M., Knohl, A., et al., 2018. Impacts of droughts and extreme-temperature events on gross primary production and ecosystem respiration: a systematic assessment across ecosystems and climate zones. Biogeosciences 15, 1293–1318.
Castellvi, F., Perez, P.J., Villar, J.M., Rosell, J.I., 1996. Analysis of methods for estimating vapor pressure deficits and relative humidity. Agric. For. Meteorol. 82, 29–45.
Chen, C., Park, T., Wang, X.H., Piao, S.L., Xu, B.D., Chaturvedi, R.K., et al., 2019. China and India lead in greening of the world through land-use management. Nat. Sustain. 2, 122–129.
Dang, C.Y., Shao, Z.F., Huang, X., Qian, J.X., Cheng, G., Ding, Q., et al., 2022. Assessment of the importance of increasing temperature and decreasing soil moisture on global ecosystem productivity using solar-induced chlorophyll fluorescence. Glob. Chang. Biol. 28, 2066–2080.
Deng, Y.H., Wang, S.J., Bai, X.Y., Luo, G.J., Wu, L.H., Cao, Y., et al., 2020. Variation trend of global soil moisture and its cause analysis. Ecol. Indic. 110.
Ding, J.Z., Yang, T., Zhao, Y.T., Liu, D., Wang, X.Y., Yao, Y.T., et al., 2018. Increasingly important role of atmospheric aridity on Tibetan alpine grasslands. Geophys. Res. Lett. 45, 2852–2859.
Doughty, C.E., Metcalfe, D.B., Girardin, C.A.J., Amezquita, F.F., Cabrera, D.G., Huasco, W.H., et al., 2015. Drought impact on forest carbon dynamics and fluxes in Amazonia. Nature 519, 78–U140.
Eamus, D., Boulain, N., Cleverly, J., Breshears, D.D., 2013. Global change-type drought-induced tree mortality: vapor pressure deficit is more important than temperature per se in causing decline in tree health. Ecol. Evol. 3, 2711–2729.
Feng, S., Fu, Q., 2013. Expansion of global drylands under a warming climate. Atmos. Chem. Phys. 13, 10081–10094.
Feng, X.M., Fu, B.J., Zhang, Y., Pan, N.Q., Zeng, Z.Z., Tian, H.Q., et al., 2021. Recent leveling off of vegetation greenness and primary production reveals the increasing soil water limitations on the greening earth. Sci. Bull. 66, 1462–1471.
Forzieri, G., Alkama, R., Miralles, D.G., Cescatti, A., 2017. Satellites reveal contrasting responses of regional climate to the widespread greening of earth. Science 356, 1140–1144.
Forzieri, G., Miralles, D.G., Ciais, P., Alkama, R., Ryu, Y., Duveiller, G., et al., 2020. Increased control of vegetation on global terrestrial energy fluxes. Nature. Climate Change 10, 356–+.
Fridley, J.D., Wright, J.P., 2018. Temperature accelerates the rate fields become forests. Proc. Natl. Acad. Sci. U. S. A. 115, 4702–4706.
Ge, W.Y., Deng, L.Q., Wang, F., Han, J.Q., 2021. Quantifying the contributions of human activities and climate change to vegetation net primary productivity dynamics in China from 2001 to 2016. Sci. Total Environ. 773.
Green, J.K., Seneviratne, S.I., Berg, A.M., Findell, K.L., Hagemann, S., Lawrence, D.M., et al., 2019. Large influence of soil moisture on long-term terrestrial carbon uptake. Nature 565, 476–+.
Hamed, K.H., 2008. Trend detection in hydrologic data: the Mann-Kendall trend test under the scaling hypothesis. J. Hydrol. 349, 350–363.
Hamed, K.H., Rao, A.R., 1998. A modified Mann-Kendall trend test for autocorrelated data. J. Hydrol. 204, 182–196.
Henderson-Sellers, A., Gornitz, V., 1984. Possible climatic impacts of land cover transformations, with particular emphasis on tropical deforestation. Clim. Change 6, 231–257.
Huang, N., Wang, L., Song, X.P., Black, T.A., Jassal, R.S., Myneni, R.B., et al., 2020. Spatial and temporal variations in global soil respiration and their relationships with climate and land cover. Sci. Adv. 6.
Jain, P., Castellanos-Acuna, D., Coogan, S.C.P., Abatzoglou, J.T., Flannigan, M.D., 2022. Observed increases in extreme fire weather driven by atmospheric humidity and temperature. Nat. Clim. Change 12, 63–+.
Kato, H., Rodell, M., Beyrich, F., Cleugh, H., van Gorsel, E., Liu, H., et al., 2007. Sensitivity of land surface simulations to model physics, land characteristics, and forcings, at four CEOP sites. J. Meteorol. Soc. Japan. Ser. II 85A, 187–204.
Koster, R.D., Dirmeyer, P.A., Guo, Z.C., Bonan, G., Chan, E., Cox, P., et al., 2004. Regions of strong coupling between soil moisture and precipitation. Science 305, 1138–1140.
Kottek, M., Grieser, J., Beck, C., Rudolf, B., Rubel, F., 2006. World map of the Koppen-Geiger climate classification updated. Meteorol. Z. 15, 259–263.
Li, Y., Piao, S.L., Li, L.Z.X., Chen, A.P., Wang, X.H., Ciais, P., et al., 2018. Divergent hydrological response to large-scale afforestation and vegetation greening in China. Sci. Adv. 4.
Libiseller, C., Grimvall, A., 2002. Performance of partial Mann-Kendall tests for trend detection in the presence of covariates. Environmetrics 13, 71–84.
Liu, W.B., Sun, F.B., 2016. Assessing estimates of evaporative demand in climate models using observed pan evaporation over China. J. Geophys. Res.-Atmos. 121, 8329–8349.
Liu, X.P., Pei, F.S., Wen, Y.Y., Li, X., Wang, S.J., Wu, C.J., et al., 2019. Global urban expansion offsets climate-driven increases in terrestrial net primary productivity. Nat. Commun. 10.
Liu, L.B., Gudmundsson, L., Hauser, M., Qin, D.H., Li, S.C., Seneviratne, S.I., 2020. Soil moisture dominates dryness stress on ecosystem production globally. Nat. Commun. 11.
Liu, Y., Shan, F.Z., Yue, H., Wang, X., 2023a. Characteristics of drought propagation and effects of water resources on vegetation in the karst area of Southwest China. Sci. Total Environ. 891.
Liu, Y., Shan, F.Z., Yue, H., Wang, X., Fan, Y.H., 2023b. Global analysis of the correlation and propagation among meteorological, agricultural, surface water, and groundwater droughts. J. Environ. Manage. 333.
Liu, Y., Yu, X.Y., Dang, C.Y., Yue, H., Wang, X., Niu, H.B., et al., 2023c. A dryness index TSWDI based on land surface temperature, sun-induced chlorophyll fluorescence, and water balance. ISPRS J. Photogramm. Remote Sens. 202, 581–598.
Madadgar, S., AghaKouchak, A., Farahmand, A., Davis, S.J., 2017. Probabilistic estimates of drought impacts on agricultural production. Geophys. Res. Lett. 44, 7799–7807.
McColl, K.A., Alemohammad, S.H., Akbar, R., Konings, A.G., Yueh, S., Entekhabi, D., 2017. The global distribution and dynamics of surface soil moisture. Nat. Geosci. 10, 100–+.
McDowell, N., Pockman, W.T., Allen, C.D., Breshears, D.D., Cobb, N., Kolb, T., et al., 2008. Mechanisms of plant survival and mortality during drought: why do some plants survive while others succumb to drought? New Phytol. 178, 719–739.
Mitchell, S.R., Emanuel, R.E., McGlynn, B.L., 2015. Land-atmosphere carbon and water flux relationships to vapor pressure deficit, soil moisture, and stream flow. Agric. For. Meteorol. 208, 108–117.
Nemani, R.R., Keeling, C.D., Hashimoto, H., Jolly, W.M., Piper, S.C., Tucker, C.J., et al., 2003. Climate-driven increases in global terrestrial net primary production from 1982 to 1999. Science 300, 1560–1563.
Oren, R., Sperry, J.S., Katul, G.G., Pataki, D.E., Ewers, B.E., Phillips, N., et al., 1999. Survey and synthesis of intra- and interspecific variation in stomatal sensitivity to vapour pressure deficit. Plant Cell Environ. 22, 1515–1526.
Peng, S.S., Piao, S.L., Zeng, Z.Z., Ciais, P., Zhou, L.M., Li, L.Z.X., et al., 2014. Afforestation in China cools local land surface temperature. Proc. Natl. Acad. Sci. U. S. A. 111, 2915–2919.
Poveda, G., 2011. Mixed memory, (non) Hurst effect, and maximum entropy of rainfall in the tropical Andes. Adv. Water Resour. 34, 243–256.
Roderick, M.L., Rotstayn, L.D., Farquhar, G.D., Hobbins, M.T., 2007. On the attribution of changing pan evaporation. Geophys. Res. Lett. 34.
Seneviratne, S.I., Corti, T., Davin, E.L., Hirschi, M., Jaeger, E.B., Lehner, I., et al., 2010. Investigating soil moisture-climate interactions in a changing climate: a review. Earth Sci. Rev. 99, 125–161.
Seo, E., Lee, M.I., Jeong, J.H., Koster, R.D., Schubert, S.D., Kim, H.M., et al., 2019. Impact of soil moisture initialization on boreal summer subseasonal forecasts: mid-latitude surface air temperature and heat wave events. Climate Dynam. 52, 1695–1709.
Song, X.W., Lyu, S.D., Wen, X.F., 2020. Limitation of soil moisture on the response of transpiration to vapor pressure deficit in a subtropical coniferous plantation subjected to seasonal drought. J. Hydrol. 591.
Stocker, B.D., Zscheischler, J., Keenan, T.F., Prentice, I.C., Peñuelas, J., Seneviratne, S.I., 2018. Quantifying soil moisture impacts on light use efficiency across biomes. New Phytol. 218, 1430–1449.
Sun, J., Qin, X.J., 2016. Precipitation and temperature regulate the seasonal changes of NDVI across the Tibetan plateau. Environ. Earth Sci. 75.
Vickers, H., Hogda, K.A., Solbo, S., Karlsen, S.R., Tommervik, H., Aanes, R., et al., 2016. Changes in greening in the high Arctic: insights from a 30 year AVHRR max NDVI dataset for Svalbard. Environ. Res. Lett. 11.
Vreugdenhil, M., Dorigo, W., Broer, M., Haas, P., Eder, A., Hogan, P., et al., 2013. Towards a high-density soil moisture network for the validation of smap in Petzenkirchen, Austria. In: IEEE International Geoscience and Remote Sensing Symposium (IGARSS), Melbourne, AUSTRALIA, pp. 1865–1868.

Wang, Y.Q., Shao, M.A., Liu, Z.P., 2010. Large-scale spatial variability of dried soil layers and related factors across the entire loess plateau of China. Geoderma 159, 99–108.
Weisheimer, A., Doblas-Reyes, F.J., Jung, T., Palmer, T.N., 2011. On the predictability of the extreme summer 2003 over Europe. Geophys. Res. Lett. 38.
Williams, A.P., Allen, C.D., Millar, C.I., Swetnam, T.W., Michaelsen, J., Still, C.J., et al., 2010. Forest responses to increasing aridity and warmth in the southwestern United States. Proc. Natl. Acad. Sci. U. S. A. 107, 21289–21294.
Yu, L.X., Xue, Y.K., Diallo, I., 2021. Vegetation greening in China and its effect on summer regional climate. Sci. Bull. 66, 13–17.
Yuan, W.P., Zheng, Y., Piao, S.L., Ciais, P., Lombardozzi, D., Wang, Y.P., et al., 2019. Increased atmospheric vapor pressure deficit reduces global vegetation growth. Sci. Adv. 5.
Zeng, Z.Z., Piao, S.L., Li, L.Z.X., Zhou, L.M., Ciais, P., Wang, T., et al., 2017. Climate mitigation from vegetation biophysical feedbacks during the past three decades. Nat. Clim. Change 7, 432–+.
Zhang, J.W., Guan, K.Y., Peng, B., Pan, M., Zhou, W., Jiang, C.Y., et al., 2021. Sustainable irrigation based on co-regulation of soil water supply and atmospheric evaporative demand. Nat. Commun. 12.
Zhang, S.R., Bai, X.Y., Zhao, C.W., Tan, Q., Luo, G.J., Cao, Y., et al., 2022a. Limitations of soil moisture and formation rate on vegetation growth in karst areas. Sci. Total Environ. 810.
Zhang, W.M., Wei, F.L., Horion, S., Fensholt, R., Forkel, M., Brandt, M., 2022b. Global quantification of the bidirectional dependency between soil moisture and vegetation productivity. Agric. For. Meteorol. 313.
Zheng, X.Y., Eltahir, E.A.B., 1998. A soil moisture rainfall feedback mechanism 2. Numerical experiments. Water Resour. Res. 34, 777–785.
Zhou, S., Zhang, Y., Williams, A.P., Gentine, P., 2019. Projected increases in intensity, frequency, and terrestrial carbon costs of compound drought and aridity events. Sci. Adv. 5.
Zhou, S., Williams, A.P., Lintner, B.R., Berg, A.M., Zhang, Y., Keenan, T.F., et al., 2021. Soil moisture-atmosphere feedbacks mitigate declining water availability in drylands. Nat. Clim. Change 11, 38–+.